AGU ADVANCING EARTH AND SPACE SCIENCE

Radio Science®

REVIEW ARTICLE
10.1029/2020RS007152

Special Section:
Special Issue of the 2019 URSI-Japan Radio Science Meeting

New Horizons in Electromagnetics in Medicine and Biology

Shoogo Ueno[1,2]

[1]Department of Biomedical Engineering, Graduate School of Medicine, University of Tokyo, Tokyo, Japan, [2]Now at, Fukuoka, Japan

Abstract Forty years of studies on bioelectromagnetics, in our laboratory, are presented to view new horizons in electromagnetics in medicine and biology. The several topics are reviewed and discussed. The review includes transcranial magnetic stimulation (TMS) of the human brain, imaging of electrical information in the brain based on magnetic resonance imaging (MRI) such as impedance MRI and current MRI, cancer therapy using magnetizable beads and pulsed magnetic fields, magnetic control of cell orientation and cell growth, and effects of radio frequency electromagnetic fields on iron ion release, and uptake from and into iron cage proteins, ferritins. These techniques are leading medicine and biology into a new horizon through the novel applications of magnetism and electromagnetics.

Key Points:

- Transcranial magnetic stimulation with a figure-eight coil for localized stimulation and deep brain stimulation by different coil configurations are proposed
- Imaging of electrical information using magnetic resonance imaging is proposed. These are magnetic resonance-based electric impedance and current imaging
- Cancer cell destruction, bone growth acceleration, iron release, and uptake from and into cage proteins, ferritins, are modulated by electromagnetic fields

Correspondence to:
S. Ueno,
ueno@athena.ap.kyushu-u.ac.jp

Citation:
Ueno, S. (2021). New horizons in electromagnetics in medicine and biology. *Radio Science*, *56*, e2020RS007152. https://doi.org/10.1029/2020RS007152

Received 8 JUL 2020
Accepted 11 MAR 2021

The copyright line for this article was changed on 20 JAN 2022 after original online publication.

1. Introduction

Bioelectromagnetics has a long history since 1600 when William Gilbert published a book "*De Magnete*," where he mentioned the relationship between human life and magnetism (Gilbert, 1600). D'Arsonval observed a magnetically induced light sensation, called "magnetophosphene" in 1896 (d'Arsonval, 1896). Modern bioelectromagnetic studies were accelerated in 1960s–1970s (Frei, 1970). In recent decades, techniques of transcranial magnetic stimulation (TMS) of the human brain and magnetic resonance imaging (MRI) have opened new horizons in brain research and medicine.

This study reviews, mostly based on our studies for 40 years, the advances in bioelectromagnetic stimulation and imaging by TMS and MRI in the first two sections. In TMS studies, principles and applications of magnetic brain stimulation are described. TMS with a figure-eight coil for a localized stimulation and deep brain stimulation by different coil configurations are proposed. Repetitive TMS or rTMS with a repetitive pulses per second has been used for therapeutic applications for the treatment of brain diseases and mental illness such as depression. To shed light on the basic mechanisms for the effects of rTMS on the brain functions, experimental studies using rat hippocampus neurons are reviewed.

In MRI studies, imaging of impedance or conductivity in the brain and imaging of electric currents in the brain are discussed toward the MRI-based neuronal current imaging, or, MR neuroimaging. Functional MRI (fMRI), diffusion tensor MRI (DTI), and molecular imaging based on MRI such as chemical exchange saturation transfer (CEST) imaging is also discussed.

In the latter sections, novel bioelectromagnetic techniques for cancer therapy and other medical applications are discussed. These include cancer cell destruction by magnetizable beads and pulsed magnetic force, bone growth acceleration by magnetic fields, and modulation of iron ion release and uptake from and into cage proteins, ferritins, by radio frequency electromagnetic fields.

Various bioelectromagnetic phenomena for different intensities and their frequencies are shown in Figure 1 (Ueno, 2015). Magnetic stimulation of the brain, that is, TMS, requires strong pulsed electromagnetic fields of 1–2 T for a short period of time (0.1–0.2 ms) to get sufficient induced electric fields for the stimulation of neurons in the brain. The magnetophosphene shows a V-shaped curve for light sensation with a minimum threshold of 10 mT at 20 Hz. Magnetic fields used in MRI systems are 0.3 T for permanent magnets and 1.5–3.0 T for superconducting magnet systems. For research purposes, ultrahigh fields MRI systems (4–9 T) are used. Magnetic orientation of biological materials is observed in 4–8 T magnetic fields. A phenomenon of parting of water is observed in an 8 T magnetic field with a field gradient of 50 T/m (Ueno & Iwasaka, 1994).

In contrast, bioelectromagnetic fields or electromagnetic fields produced from the living system are extremely weak, 10^{-15}–10^{-11} T or 1 fT to 10 pT order of magnetic fields, buried with urban noise. These fields are measured

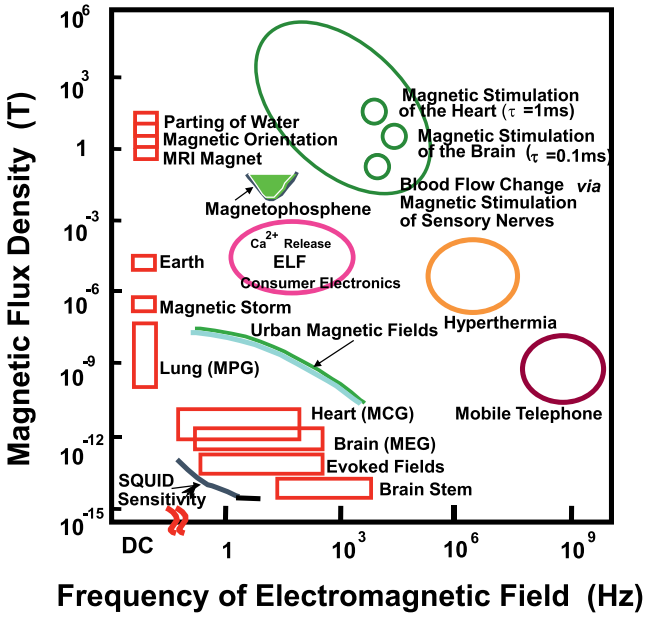

Figure 1. Various bioelectromagnetic phenomena observed or used at different frequencies (Hz) and field intensities (T).

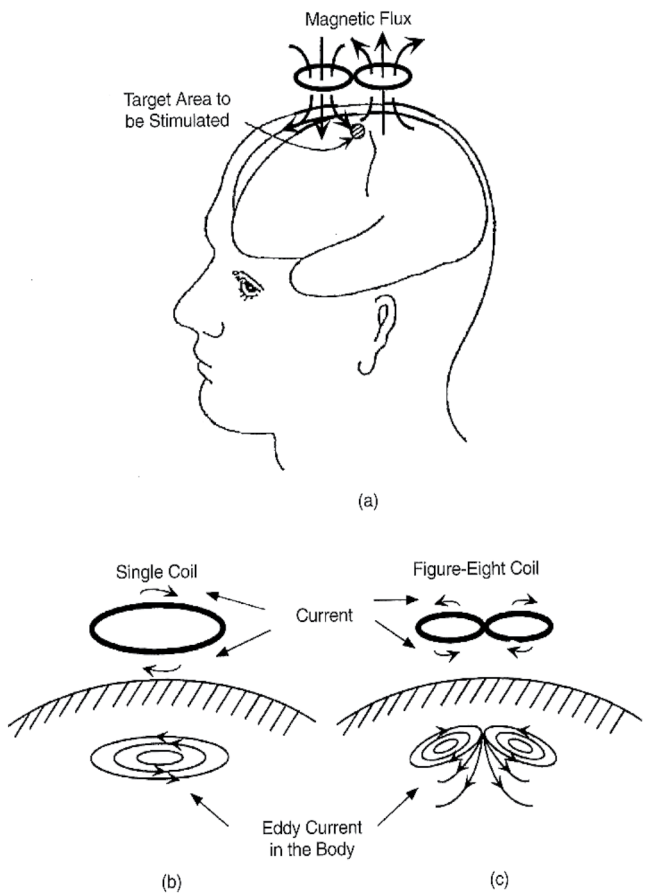

Figure 2. Principle of transcranial magnetic stimulation.

by superconducting quantum interference device (SQUID) systems in a magnetically shielded room.

The studies of possible health effects of magnetic and electromagnetic fields are important to assess and to make guidelines not only for medical usage but also for mobile telephony. Biological effects of electromagnetic fields related to MRI are discussed with three types of fields: static magnetic fields, time-varying magnetic fields generated by gradient coils, and thermal effects generated by radio frequency electromagnetic fields at the resonant frequency. The guidelines are issued by the international commission on nonionizing radiation protection (ICNIRP) and other international and national institutions.

2. Brain Stimulation by Transcranial Magnetic Stimulation

2.1. Principles of Transcranial Magnetic Stimulation

TMS is a technique to stimulate the human brain transcranially by a coil positioned on the surface of the head. The coil is driven by pulsed electric currents with several 100 A and about 50–150 μs duration, to produce transient magnetic fields of about 1 T, which results in generating induced electric fields in the brain. The induced electric fields stimulate the neurons in the brain when the electric fields exceed the threshold of nerve excitation or inhibition. TMS was first reported by Barker et al. (1985).

The successful brain stimulation by TMS made a strong impact on the scientific community. By their method, however, it was difficult to stimulate the targeted areas in the brain locally. A method of localized brain stimulation with a figure-eight coil was proposed by Ueno et al. (1988), and stimulation of the human motor cortex within a 5-mm resolution was realized (Ueno et al., 1990).

Figure 2 shows the principle of TMS using a figure-eight coil to stimulate a target area in the brain. The principle of localized stimulation by a figure-eight coil is to concentrate induced electric currents or electric fields in the target area by a pair of coils which generate oppositely directed magnetic fields around the target. The induced currents of two vortices produced by the two coils merge at the target, where the neurons can be stimulated. The computer simulation shows that the current density at the target is three times higher than current densities at nontargeted areas at the same depth. Since the induced currents at the target where two vortices merge flow in the direction perpendicular to the long axis of the figure-eight coil, vectorial stimulation can be achieved. By this method, we obtained functional maps in the human motor cortex related to the hand and foot areas, and we found that the functional maps have vectorial characteristics for brain stimulation. In other words, neurons in the brain which innervate muscles in the fingers and toe have optimal directions for the brain stimulation (Ueno et al., 1990).

Figure 3 shows the functional mapping of the human motor cortex obtained by TMS with a figure-eight coil (Ueno, 1994; Ueno et al., 1990). The distance between grid points is 5 mm. The arrows show optimal directions for brain stimulation in the motor cortex related to the hand and foot areas. The regional and directional dependences of neuronal excitability reflect the structures of gyri and sulci of the brain.

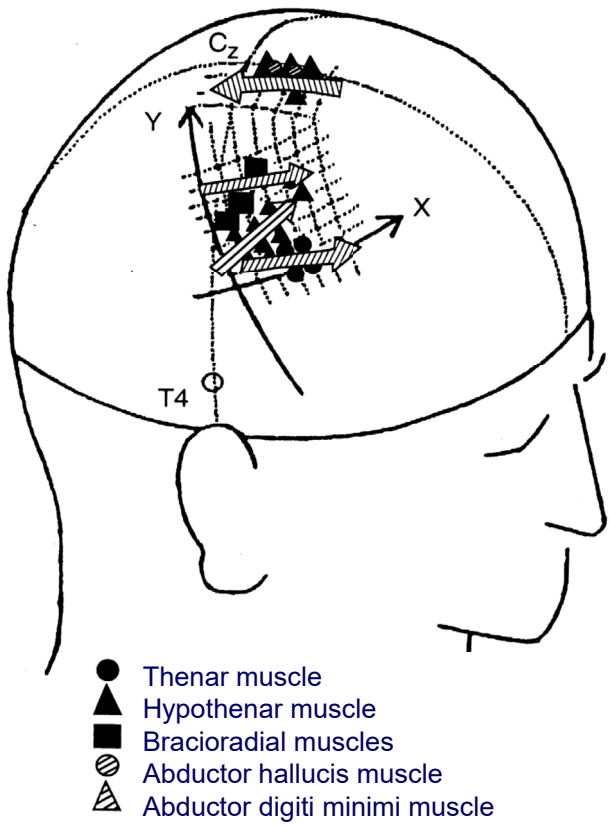

Figure 3. Functional distribution of the human motor cortex related to the hand and foot areas. The arrows show optimal directions of induced currents for brain stimulation. The distance between grid points is 5 mm.

TMS with a figure-eight coil is now used worldwide in cognitive brain research and medicine because this method is useful in investigating functional organization in the brain noninvasively and getting so-called virtual lesions in the brain for a short period of time. Functional mapping of the brain is applied also for neurosurgery (Ueno & Fujiki, 2007). Identifying motor and language areas before surgery is important for preventing damage to these areas. TMS-guided monitoring of these areas during surgery is available, because TMS can be used even in an operating room, and identification using TMS is totally noninvasive. For the surgical planning, MRI can be used to image guide the brain location with information on the accuracy of the placement before surgery. Then, during surgery, putting a figure-eight coil on the surface of the cortex, real-time monitoring of motor and language areas is carried out by the TMS.

2.2. Toward Deep Transcranial Magnetic Stimulation

TMS with a figure-eight coil has a powerful tool in stimulation of the cortex, but it has a disadvantage in deep brain stimulation. For the treatment of mental illness such as depression, deep brain stimulation is needed to stimulate important nuclei related to the award circuits which are localized in the deeper part in the brain. Several methods for deep brain stimulation by different coil configurations are proposed (Crowther et al., 2011; Lu and Ueno, 2015, 2017; Roth et al., 2002; Zangen et al., 2005).

We evaluated these coil configurations from a view point of focality, obtaining three-dimensional distributions of induced electric fields in the brain. Based on the evaluation, we proposed a method of deep brain stimulation using three coaxial circular coils, in which direction of injecting currents into the middle coil is reversed compared to the currents into two outer coils. The simulation results show that focality is improved in the proposed method compared with other coil configurations (Lu and Ueno, 2015, 2017). For example, the ratio of induced electric field in deep brain regions to shallow brain areas is 2.07 for the proposed coil configuration, which is better when compared to that of 1.46 for one circular coil or 1.31 for two circular coil configurations. The calculated results show that we obtain a focal brain stimulation of a brain tissue volume of 2,000 mm^3 or 13 mm in cubic size with induced electric field over 100 V/m at the depth 70–90 mm from the vertex of the head model. This is better focality compared to 8,000 mm^3 for one circular coil and 10,000 mm^3 for two circular coils at the same depth. The method using three coaxial circular coils, however, has the limits on accuracy of placement and minimum excited brain tissue in deeper parts of the brain. It is noteworthy that Grossman et al. proposed a technique for deep brain stimulation using RF temporal interference (Grossman et al., 2017). Further studies are needed for deep TMS with better focality.

2.3. Changes in Functions of Hippocampus Neurons by Repetitive TMS

rTMS is used for therapeutic applications such as treatments of brain diseases and mental illness such as Parkinson's disease and depression. However, the mechanisms underlying the effects of rTMS on brain function is unknown. A number of animal studies testing the basic mechanisms of rTMS-induced alternations of neurotrophic factors, gene expression, and changes in plasticity have been conducted. The experiments suggest that there is a strong evidence that the expression of certain genes such as the immediate early gene, astrocyte-specific glial fibrillary acidic protein (GFAP) messenger ribonucleic acid (mRNA) and brain-derived neurotropic factor (BDNA) are altered by rTMS (Fujiki & Stewart, 1997; Muller et al., 2000). The effects of rTMS on neuronal electric activities in the rat hippocampus were studied, focusing on long-term potentiation (LTP) by our group (Ogiue-Ikeda, Kawata, &Ueno, 2003; Ogiue-Ikeda et al., 2005). A series of the studies suggest that rTMS modulates or contributes to memory function, learning and memory processes, neuronal plasticity, prevention of neurons against injury, recovery of injured neurons, and acquisition of tolerance against cerebral ischemia. Further

studies are needed for clinical application based on the rTMS-induced neuromodulation and neurorehabilitation medicine.

3. Bioelectromagnetic Imaging by Magnetic Resonance Imaging

3.1. Advances in Magnetic Resonance Imaging

MRI is a technique to obtain images based on NMR signals generated by nuclei under a strong magnetic field. The MRI technique was demonstrated by Lauterbur in 1973 (Lauterbur, 1973). The principle of imaging is to introduce gradient coils to produce linearly increased or decreased gradient magnetic fields in addition to the main static magnetic fields. The resonant frequency, or, Larmor frequency of proton in the tissues varies with the position, which gives us the spatial information in the space of the Fourier Transformation (FT). Mansfield introduced a new pulse sequence system, called echo planar imaging (EPI), to obtain imaging in a very short time (Mansfield, 1977). In MRI diagnosis, clinically useful images are obtained by changing parameters such as spin-spin relaxation time T_2 and spin-lattice relaxation time T_1. T_1-weighted image suppresses signals of blood and cerebrospinal fluids, whereas T_2-weighted image enhances signals of blood and cerebrospinal fluids.

Because of its variety of potential abilities, MRI has been developed in different variational applications such as functional MRI (fMRI), diffusion tensor MRI (DTI), MRI-based impedance and current imaging, molecular MRI, and so on. Ogawa invented fMRI based on blood oxygenation level dependent (BOLD) effects (Ogawa et al., 1990), and demonstrated the usefulness of fMRI using human subjects (Ogawa et al., 1992). Using the BOLD effect, fMRI is able to detect the functional signals in the brain related to the change in magnetic susceptibility of oxyhemoglobin (diamagnetism) and deoxyhemoglobin (para-magnetism) in the blood. The BOLD effect reflects on the local spin-spin relaxation T_2*, and the changes in T_2* are detected as the functional signals associated with neuronal electrical activities. fMRI has been used in a variety of fields from basic research to cognitive and social sciences.

Diffusion magnetic resonance imaging (dMRI) measures the diffusion of water molecules along different dimensions (Stejskal & Tanner, 1965). Anisotropy of diffusion in the nervous tissues led to the development of clinically important tool called tractography, a noninvasive method for visualizing white matter bundles in vivo that is now indispensable for presurgical planning. Recent advances in dMRI and DTI have powerful tools to visualize structures of neuronal fibers and neuronal networks in the human brain.

3.2. Magnetic Resonance Imaging of Electric Impedance

Conventional MRIs give no information of electrical properties such as electric impedance and currents in the brain. Imaging of impedance or conductivity in the brain, called impedance MRI has been studied in our group. We proposed three different methods for impedance or conductivity MRI: a large flip angle method to obtain imaging at resonant frequency (Ueno & Iriguchi, 1998), a method to obtain conductivity-enhanced imaging at an arbitrary frequency by inserting additional time-varying field parallel to the main static field (Yukawa et al., 1999), and a conductivity MRI based on diffusion tensor MRI (Sekino et al., 2005; Sekino, Yamaguchi, et al., 2009). Using the relationship between the self-diffusion coefficient of water and live tissue conductivity, a method is proposed to map conductivity, which is characterized by being able to make measurements including conductivity anisotropy.

Figure 4 shows the results obtained by the diffusion tensor conductivity MRI of the human brain. The signals in corpus callosum exhibit high anisotropy due to the alignment of neuronal fibers (Sekino et al., 2005). Regions with high anisotropic conductivity are also observed in the white matter. In other words, the white matter contains several regions where conductivities are highly dependent on the direction in the motion probing gradient (MPG). In the lower parts in Figure 4, the image of the mean conductivity (MC) is shown in the left side, and the image the anisotropy index (AI) is shown in the left side.

Going back to the principle of MRI, magnetization rotates at a Larmor frequency, or, resonant frequency proportional to the strength of an applied magnetic field, which is reflected in the frequency and phase of magnetic resonance signals. Focusing on this, it is possible to find the internal magnetic field distribution of the object from MRI signals. Magnetic field distribution is affected by the values of electromagnetic properties, such as, current, conductivity, permittivity, and susceptibility, and thus it is possible to visualize these electrical properties using

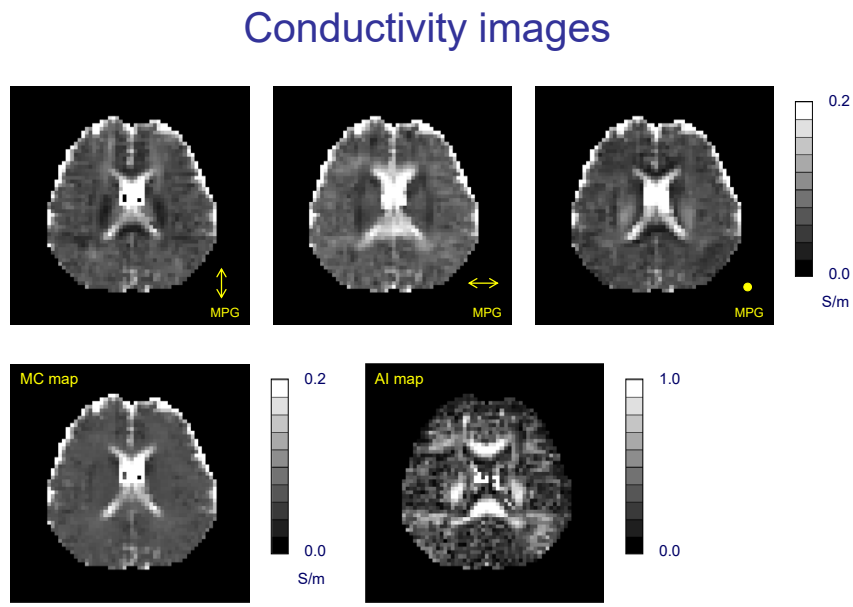

Figure 4. Conductivity images of the human subject obtained by the diffusion MRI. In upper three figures, images from the left to the right are the estimated conductivity distributions in the anterior-posterior, right-left, and superior-inferior directions, respectively, in the MPG. In the lower two figures, image of the MC in the left side, and image of the AI in the right side, are shown.

MRI. If it is able to combine MRI of electrical properties and DTI in order to get in vivo fiber tractography with information of electrical properties, it will be useful in diagnosis of brain diseases. Furthermore, if accurate and precise high-resolution maps of the electrical properties of tissues in the brain and other organs could be achieved, the potential applications could be expanded. For example, techniques have been reported for determining the conductivity and permittivity of a body region based on RF field distribution, and clinical applications of this technique are expected based on the need to evaluate specific absorption rate (SAR) in high-field MRI.

3.3. Magnetic Resonance Imaging of Electric Currents

Detection of weak magnetic fields arising from neuronal electrical activities using MRI is a potentially effective method for functional imaging of the brain. Neuronal magnetic fields observed at the surface of the head are very weak, for example, smaller than, 10^{-12} T or 1 pT. Magnetic fields attenuate with the distance from neurons. Thus, the strength of neuronal magnetic fields in close proximity to the neurons should be much higher than the one measured on the scalp.

We proposed a method of current imaging based on MRI using gradient magnetic fields with different polarities to detect neuronal fields and to eliminate signal variations resulting from other effects (Kamei et al., 1999). Using a 1.5-T MRI system, we obtained the neuronal current imaging of the human somatosensory cortex responded to tapping of the right hand's middle finger and thumb. However, there has been a debate about the feasibility of this method because the magnetic fields arising from neurons are very weak, and the signal was too small. Toward neuronal current imaging by MRI, we basically studied the possibility of electrical current imaging based on magnetic resonance as follows:

In the first step, we investigated the theoretical and practical limits of sensitivity for detecting weak magnetic fields. The limit of sensitivity was estimated from the signal-to-noise intensities in MRI. The signal intensity was calculated with parameters that are commonly used in measurements of the human brain. The noise due to the head was calculated using the finite element method (FEM). The results show that the limit of sensitivity is 10^{-8} T for measurements of the human brain (Hatada et al., 2005). Although this implies that the MRI has sufficient sensitivity at voxels located close to neurons, the details of the influence of neuronal magnetic fields on MRI signals at these voxels remain to be understood.

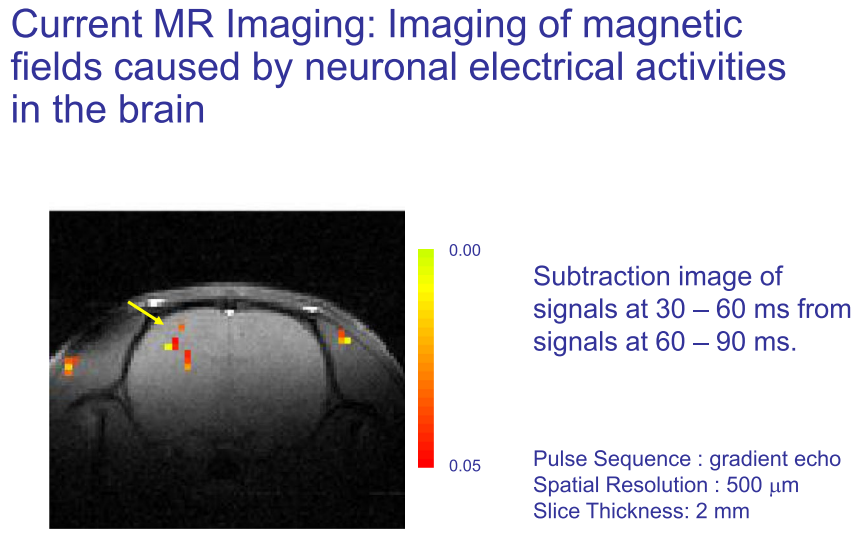

Figure 5. Detection of magnetic fields arising from neuronal activities obtained by a gradient echo sequence using a 4.7 T MRI. The figure shows the functional image of a rat brain at a slice which includes the somatosensory area determined by a T_1-weighted image. The scale shows p-values. The signal intensities from the images obtained at adjacent time points were compared after electrical stimulation of the sciatic nerves. The time "30–60, 60–90 ms" means a comparison between the images excited at 30 ms (and acquired at 60 ms) and the image excited at 60 ms (and acquired at 90 ms). The position pointed by an arrow is the somatosensory area in the right hemisphere responded to electrical stimulation of the sciatic nerves on the left hindlimb.

In the second step, we theoretically estimated the influence of neuronal magnetic fields on the MRI using a current dipole model. Neuronal magnetic fields were modeled using a current dipole formula, and the resulting magnetic resonance signals were calculated for a voxel located close to the dipole. We estimated the current dipole strengths of 4, 8, and 12 nA-m, respectively generating magnetic fields of 1, 2, and 3 pT at 20 mm from the dipole (Sekino, Ohsaki, et al., 2009). A current dipole strength of 12 nA-m resulted in the maximum signal drop of 0.6%. The signal drop of 0.6% is sufficiently detectable. Evoked or spontaneous magnetic fields measured on the scalp (measurement distance $r = 20$–40 mm away from the current source) by human magnetoencephalography (MEG) are on the order of 10^{-12} T for spontaneous magnetic fields or 10^{-13} T for evoked magnetic fields. These fields primarily result from a synchronized activity of postsynaptic currents in a large number of the pyramidal neurons of the cortex. If the current dipole sources of these neuronal magnetic fields are order of 10 nA-m, neuronal current MRI will be achieved.

In the third step, we measured MRI signals in the rat brain responded to electrical stimulation of the sciatic nerves. The sciatic nerve was exposed through a skin incision of approximately 30 mm on the left hindlimb, and a pair of platinum wire electrodes was attached to the sciatic nerves for electrical stimulation. Pulsed electrical stimulations were applied to the wire electrodes with a duration of 0.1 ms and a repetition rate of 3 pulses/s. The imaging slice with a thickness of 2 mm was located on the somatosensory cortex. Anatomical locations for detected changes in the functional images were identified by using a T_1-weighted image which was obtained by using a spin echo sequence. Functional images were obtained using a gradient echo sequence. Transient changes in the signal intensity resulting from neuronal activities in the rat brain were measured using a 4.7-T MRI system (Sekino, Ohsaki, et al., 2009). The excitation pulses were applied every 30 ms at 10 time points (0, 30, 60, …, and 270 ms) after electrical stimulation of the left sciatic nerves. The signal intensities of functional images obtained with and without stimulation were statistically compared using a Student's *t*-test.

A transient decrease in the signal intensity was found at 30–60 ms after stimulation. This result is consistent with a local change in the magnetic field resulting from neuronal activities. As shown in Figure 5, the images were compared at adjacent time points to investigate temporal changes. A significant difference was observed between 30–60 and 60–90 ms in the right somatosensory area, which suggests that these effects arose temporarily from neuronal magnetic fields. The activated areas, however, show not only the somatosensory cortex but also other areas of the brain. This is perhaps caused by noise in images because the sensitivity of present MRI is not

sufficiently high above the strength of neuronal magnetic fields. The signal-to-noise ratio (SNR) should be improved in future works. Further studies are needed for the reliable current MRI of human subjects (Ueno, 2020).

Conventional tools of functional imaging provide a part of the brain information, for example, fMRI provides a spatial distribution of the activities, and MEG provides potential changes of the activities. Our proposed method visualizes the spatiotemporal changes in dynamic brain activities, which will open a new horizon in functional brain research.

3.4. Molecular Imaging Based on Magnetic Resonance Imaging

CEST imaging is one of the novel MRI-based molecular imaging modalities, and its usefulness was first demonstrated by Ward and Baraban in 2000 (Ward & Balaban, 2000). CEST allows for the imaging of low-concentration endogenous and exogenous molecules with spatial resolution comparable with those in imaging obtained by conventional MRI. In addition, CEST imaging has the potential to provide physiological information which includes pH and glucose concentration. CEST contrast is achieved by applying a saturation pulse at the resonant frequency of a slow-intermediate exchanging proton site of endogenous or exogenous CEST agents. Amide proton transfer (APT) imaging is a specific type of endogenous CEST imaging technique proposed by Zhou et al. (2003). This method enables the semi-quantitative measurement of amide protons (-NH) in intrinsic mobile proteins and peptides, which have a specific resonant frequency 3.5 ppm downfield to that of water. The chemical shift in CEST imaging is defined as the frequency shift from the offset frequency of water molecules. In CEST imaging using a 3-T MRI, for example, the resonant frequency of water is 127.73 MHz, and the chemical shift of 3.5 ppm is 447 Hz. Because this resonant frequency is sufficiently remote from that of water, and amide protons are relatively abundant in tissue, especially in tumors, APT imaging is considered the most clinically relevant type of CEST imaging. Chemical shift 3.5 ppm in APT is larger compared with other proteins; 0.5–1.5 ppm in glycogen (glycol CEST), 0.9–1.9 ppm in glycosaminoglycan (gag CEST), 3.0 ppm in glutamate (glu CEST), and 0.6 ppm in myo-inositol (MI CEST). Lee et al. reported the in vitro measurements of the CEST effects from endogenous CEST agents that are commonly found in biological tissues and organs, at magnetic fields of 3 and 7 T and under various pH conditions (Lee et al., 2015).

There are many problems and limits for clinical use of CEST imaging that should be solved. These include the low SNR under the restriction of SAR and duty cycle, complexity in data analysis caused by various factors such as nonspecific magnetization transfer (MT) effect and the nuclear Overhauser effect (NOE), and optimization of pulse sequences, in particular, selection of intensity and duration of saturation pulses. CEST imaging requires a sufficiently slow exchange on the magnetic resonance time scale to allow selective irradiation of the protons of interest. As a result, magnetic radiolabeling is not limited to radio frequency saturation but can be explained with slower frequency-selective approaches such as inversion, gradient dephasing, and frequency radiolabeling (Van Zijl & Yadav, 2011). By solving the difficulties in CEST imaging, many approaches to clinical diagnosis are reported (Togao et al., 2014).

The APT effect is most often quantified as the asymmetry of the MT ratio, MTR_{asym} at 3.5 ppm: MTR_{asym} (3.5 ppm) = $(S_{-3.5\ ppm} - S_{3.5\ ppm})/S_0$, where, $S_{-3.5\ ppm}$ and $S_{3.5\ ppm}$ are the signal intensities at −3.5 and 3.5 ppm, respectively, and S_0 is the unsaturated signal intensity. The MTR_{asym} value at 3.5 ppm is widely used as an approximate index of APT signal intensity and is often called APT-weighted signal intensity (APTWSI). APT-weighted images are obtained by performing a voxel-wise mapping of this index. The usefulness of the APTWSI in grading glioma has been confirmed by several research groups. For examples, APTSWI can differentiate high-grade (grades III and IV) glioma from low-grade (grade II) ones with a sensitivity of 93% and a specificity of 100%, and APTSWI is superior to the apparent diffusion coefficient (ADC) and relative cerebral blood flow volume in distinguished malignant glioma without intense contract enhancement from benign glioma (Togao et al., 2014; Yoshiura, 2020).

The clinical translation of APT imaging has been progressing, especially regarding brain tumors, and is currently expanding to include head and neck, abdomen, and chest pathologies. CEST imaging of pH could have a significant impact on the clinical management of acute brain infarction and malignant tumors but requires further technical refinement toward clinical use (Yoshiura, 2020). CEST imaging has opened a new horizon in MRI-based molecular imaging.

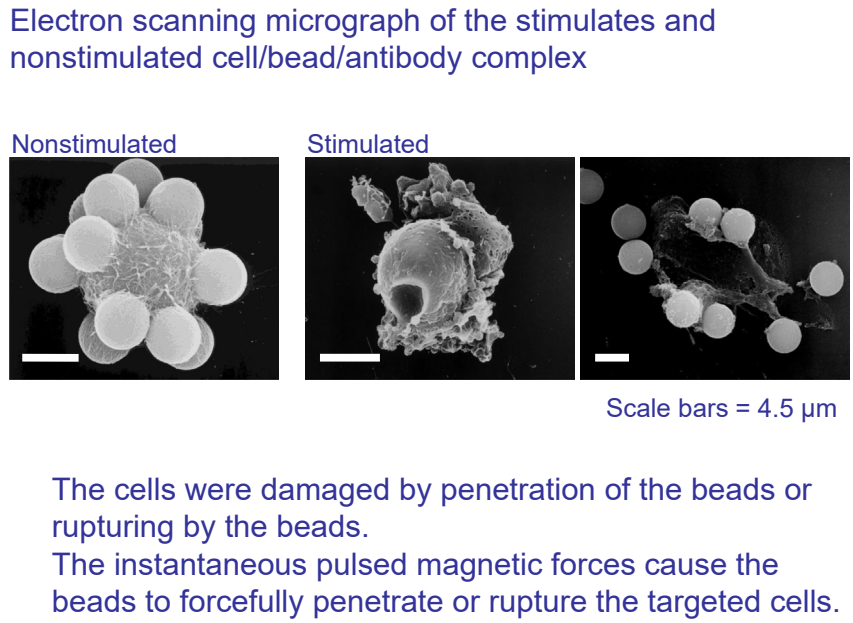

Figure 6. Physical destruction of leukemic cells by electromagnetic pulses and magnetizable beans. Figures, from the left to right, are a scanning electron micrograph of TCC-S cell combined with beads by an antigen-antibody reaction, that is, the cell/bead/antibody complex without electromagnetic stimulation, the cell/bead/antibody complex damaged by a penetration of bead into the cell, and damaged cell by ruptured with electromagnetic stimulation.

4. Cancer Therapy by Magnetizable Beads and Pulsed Magnetic Force

Treatment modalities for eradicating cancer cells using heat from electromagnetic waves and ultrasonic cavitation are widely investigated. Irradiation of only targeted tumors without risking damage to normal tissues, however, is not feasible using either modality. Furthermore, these modalities are also ineffective for deep-seated tumors, in which only invasive methods using implanted antennas are available.

We proposed a new method to destroy targeted cancer cells physically by using pulsed magnetic forces and magnetizable beads (Ogiue-Ikeda, Sato, & Ueno, 2003). Magnetic force acting on magnetic materials move the materials along magnetic field gradients. Superparamagnetic iron oxide (SPIO) beads or dynabeads™ are introduced as magnetic materials. The dynabeads™ are monosized, superparamagnetic, microporous particles with narrow pores, in which magnetizable materials, that is, SPIO materials are distributed in the pores throughout the whole volume of the particles. We used TCC-S leukemic cells, which were established from a patient with chronic myelogenous leukemia in myeloid crisis. TCC-S leukemic cells were combined with the magnetizable beads by an antigen-antibody reaction. The CD33 antigen was expressed on the surface of TCC-S cells. After combination, the cell/beads/antibody complexes were placed on a magnet for aggregation. The targeted cells were then stimulated by a coil that produced pulsed magnetic fields of 2.0 T with a field gradient of 100 T/m.

As shown in Figure 6, the cancer cells were destroyed by the penetration of the beads into the cancer cells or the rupturing of cancer cells by the beads. In contrast, the noncell/bead/antigen complexes, or, the cell-bead mixtures without an antigen-antibody reaction were not damaged by magnetic stimulation. The absence of heat and micro-bubbles makes this a potentially viable treatment modality for solid tumor type cancers as well as leukemia in which cells are distributed throughout the whole body.

Application of this method for the treatments of solid cancer cells will have a difficulty in producing high gradient magnetic fields over a distance that could accommodate a person's body. Instead, this method will be firstly applied to the treatment of blood cancers such as leukemic cells flowing in the blood vessels. A part of blood flows is bypassed outside the body or is detoured near the surface beneath the skin, and the blood flow is exposed to pulsed magnetic force to destroy the leukemic cells. In vivo studies using small animals are needed to accumulate basic data for clinical use.

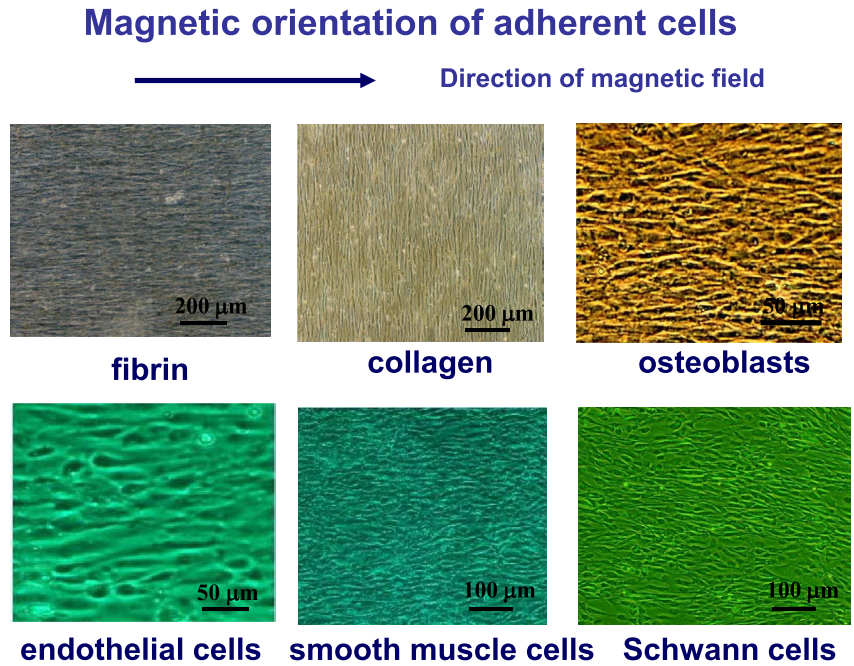

Figure 7. Magnetic orientation of fibrous proteins and adherent cells. Fibrin, osteoblast cells, blood endothelial cells, smooth muscle cells, and Schwann cells orient in parallel to the direction of magnetic fields. In contrast, collagen fibers orient in the direction perpendicular to the magnetic fields. Magnetic field intensity is 8 T in fibrin, collagen, osteoblasts, smooth muscle cells and Schwan cells, and 14 T in endothelial cells.

5. Magnetic Control of Cell Orientation and Cell Growth

We observed a phenomenon, in which water is parted when exposed to an 8 T magnetic field with a gradient of 50 T/m (Ueno & Iwasaka, 1994). We named this phenomenon "Moses effect" from the description in the Exodus. It is possible to apply the Moses effect to bioengineering and medicine, for example, by manipulating biological cells and materials, controlling spatial distributions of biomaterials and biopolymers using external magnetic fields with a high field gradient.

On the other hand, spatially homogeneous magnetic fields, or, magnetic fields with low field gradients produce a magnetic torque on the materials where a magnetic orientation is observed. Magnetic orientation is a phenomenon where biological materials align in the direction in parallel or perpendicular to magnetic fields when the materials are exposed to magnetic fields. Torbet et al. reported magnetic orientation of fibrin gels in strong magnetic fields (Torbet et al., 1981). When diamagnetic materials with a high anisotropy in magnetic susceptibility are exposed to magnetic fields, the materials align in the direction either in parallel or perpendicular to the magnetic fields depending on the anisotropy of magnetic susceptibility of the materials.

As shown in Figure 7, we observed the magnetic orientation of adherent cells such as osteoblast cells, vascular endothelial cells, smooth muscle cells, human kidney cells, and Schwann cells under 8 or 14 T magnetic field exposures. Fibrin, osteoblast cells, blood endothelial cells, smooth muscle cells, and Schwann cells orient in parallel to the direction of magnetic fields. In contrast, collagen fibers orient in the direction perpendicular to the magnetic fields. These effects are important for potential medical and bioengineering applications such as tissue repair, artificial bone development, etc.

We studied the effects of strong magnetic fields on bone formation in both in vivo and in vitro systems (Kotani et al., 2002). After 60 h of exposure to an 8 T magnetic field, cultured mouse osteoblastic MC3T3-E1 cells were transformed to rod-like shapes and were oriented in the direction parallel to the magnetic field. The magnetic field exposure did upregulate cell differentiation and matrix synthesis. We observed that in mice, the magnetic field stimulated ectopic bone formation in and around an implanted pellet containing bone morphogenetic protein 2 (BMP-2) and that the orientation of bone formation was parallel to the magnetic field.

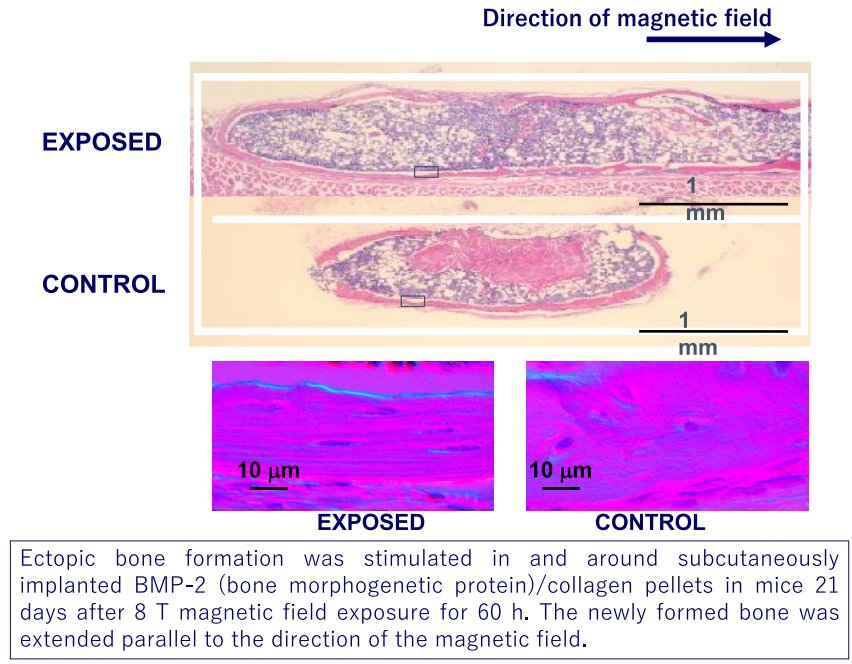

Figure 8. Bone growth acceleration by magnetic fields. Histological analyses of the magnetic field effects on bone formation in and around the BMP-2 (bone morphogenetic protein)/collagen pellets implanted subcutaneously in mice. Twenty-one days after 60 h of 8-T magnetic field exposure, the samples of BMP-2/collagen pellet were observed by light microscopy (for bone structures in the upper figures) and by differential interference contrast microscopy (for tissue structures in the lower figures). The arrow indicates the direction of the magnetic fields. Bone growth was accelerated by magnetic field exposures (Kotani et al., 2002).

As shown in Figure 8, we succeeded in bone growth acceleration using magnetic fields. Strong magnetic fields have the potential to stimulate bone formation as well as regulate its orientation in both in vitro and in vivo models. It is noteworthy that the tissues in the boundary between inside and outside of the bone orient in the direction of magnetic fields. The magnetically induced beautiful alignment of the boundary tissues accelerated the bone growth.

We also studied nerve regeneration in vivo using rats under the condition of transected sciatic nerves. We observed a difference in sciatic nerve regeneration 12 weeks after neurotomy when control and magnetically treated (exposed to 8 T magnetic field) groups were compared. The results suggest that a magnetically aligned collagen structure in silicon tube filled with type I collagen can guide the growth cone and nerve axon, resulting in accelerated nerve regeneration (Eguchi et al., 2015).

Ultra-high field MRI systems for human subjects are used in several institutions in the world. Using such MRI systems, exposures to 4–8 T magnetic fields are available also for the treatment purposes. For potential regenerative medicine and treatments of bones, nerves, blood vessels, and other tissues in peripheral parts in the body, small devices with ultra-high magnetic fields will be hopefully developed. New approaches to therapeutic treatments using ultra-high magnetic fields will open a new horizon in medicine and biology.

6. Effects of Radio Frequency Electromagnetic Fields on Iron Release and Uptake From and Into Iron Cage Proteins, Ferritins

We have explored the effects of radio frequency electromagnetic fields on naturally occurring magnetic nanoparticle-protein biosystems, using iron cage proteins, ferritins. Ferritin is a protein composed of a roughly spherical, polypeptide cage inside of which is a ferrihydrite nanoparticle formed from the absorption, oxidation, and incorporation of Fe^{2+} ions. The resulting nanoparticle is superparamagnetic at room temperature, which leads to a magnetization lag and power loss when exposed to alternating electromagnetic fields at a high enough frequency. The energy generated by the nanoparticle is dissipated to the environment, and we have found that this affects the

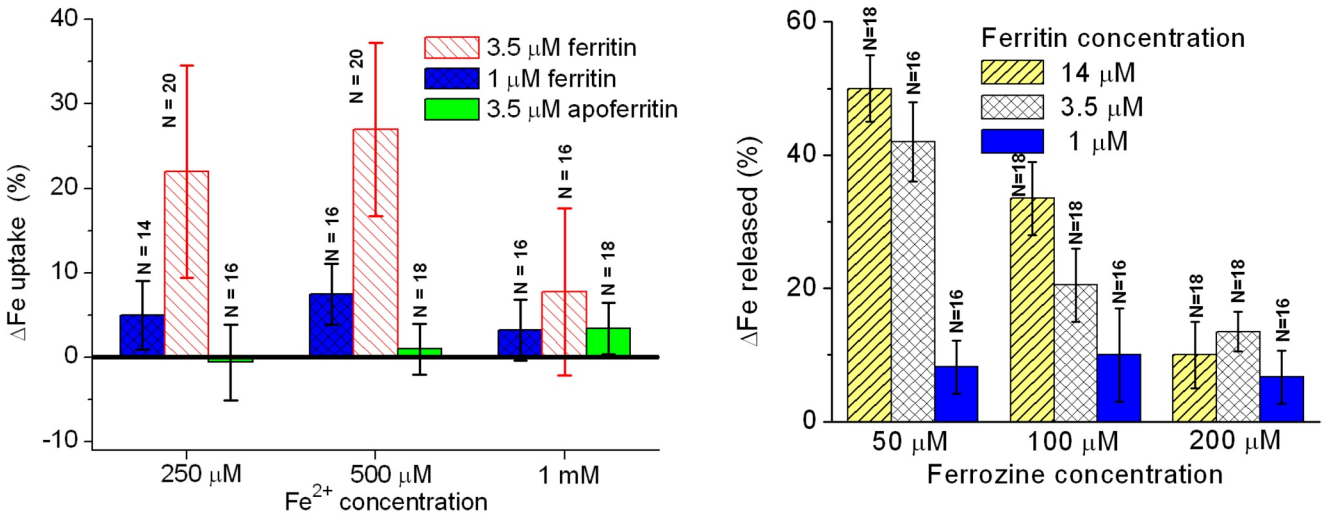

After a 5 hours exposure to fields of 1 MHz and 30 μT, the iron uptake and release are reduced. ΔFe uptake/released = (Fe $|_{control}$-Fe $|_{exposed}$) / Fe $|_{control}$, with Fe $|_{control}$ and Fe $|_{exposed}$ the iron chelated/uptaked after 1 hour in control and exposed samples, respectively.

Figure 9. Effects of radio frequency electromagnetic fields on iron uptake and release versus concentrations. The samples were exposed to radio frequency magnetic fields of 1 MHz and 30 μT for 5 h before the measurement of chemical concentrations. The error bars are calculated as the standard error of the mean. Figure at the left side shows changes in iron uptake after exposure to RF field as a function of the chemical concentration of iron cations and ferritin. The figure at the right side shows changes in iron release after exposure to RF field as a function of chemical concentrations of ferritin and ferrozine as a chelating agent. By the exposures to RF fields at 1 MHz and 30 μT, iron uptake is reduced 30% when ferritin concentration is 3.5 μM and Fe^{2+} concentration is 500 μM, and iron release is reduced 50% when ferritin concentration is 14 μM and ferrozine concentration is 50 μM. In contrast, in apoferritin, that is, in cage protein without inner ferrihydrite nanoparticles, the effect is not significant. That is, RF electromagnetic fields have no effect on apoferritin.

functioning of the protein. When an iron chelator (ferrozine in our experiment) is added to a ferritin solution, the chelator goes into the protein cage and moves one iron ion from the nanoparticle.

We studied the effects of RF electromagnetic fields on iron ion release and uptake from and into the ferritins. As shown in Figure 9, we observed that the amount of iron chelated after 1 h is reduced by up to a factor of 3 in proteins previously exposed to RF electromagnetic fields of 1 MHz and 30 μT for 5 h (Céspedes & Ueno, 2009; Cespedes et al., 2010). The error bars in Figure 9 are calculated as the standard error of the mean.

We consider the iron chelation speed or iron release when using ferrozine as a reducing and chelating agent. When ferrozine is added to a solution of ferritin proteins, the molecule may penetrate the protein cage through the threefold symmetry points. The protein is then well protected against strong, negatively charged, iron chelation such as ferrozine. When using ferrozine as chelating agent, we found that samples previously exposed to RF electromagnetic fields of 1 MHz of 30 μT released up to 40%–50% less iron than control samples. We define the electromagnetic field effect on the change of iron release as

$$\Delta Fe_{released} = \left(Fe_{released|control} - Fe_{released|exposed}\right) / Fe_{released|control},$$

where $Fe_{released}|_{control}$ and $Fe_{released}|_{exposed}$ are the total iron released 1 h after adding the chelating agent discounting the initial burst in control and exposed samples, respectively. This effect was dependent on several parameters, including the amplitude and frequency of electromagnetic fields, the exposure time, the ferritin and ferrozine concentration, and the pH of the solution.

The variation of the electromagnetic field effect with chemical concentrations of ferrozine and ferritin (Figure 9 right) can be explained as due to pH variations and changes in the intermolecular interactions. The pH of the ferritin solution decreases when the acidic ferrozine is added, which will result in iron reduction and increased rates of release. On the other hand, the protein itself and the NaCl solution in which it is dissolved act as a buffer to the pH

change. High rates of iron release due to lower pH will affect both control and exposed samples, decreasing the electromagnetic field effect. The reason for smaller effects at lower ferritin concentration (1 μM) may also be due to the buffer effect of the proteins or to a decrease in protein interactions, which being energetically weaker, on the order of 8 kJM^{-1} instead of 300 kJM^{-1} for protein subunit interaction (Stefanini et al., 1996; Yau et al., 2000), would be expected to be more affected by the irradiated energy.

Figure 9 (left) shows the decrease in iron uptake into ferritin after exposure to RF electromagnetic fields as a function of the chemical concentrations of iron cations Fe^{2+} and ferritin. As described in the case for iron release, we define the electromagnetic field effect on the change of iron uptake as

$$\Delta Fe_{uptake} = \left(Fe_{up|control} - Fe_{up|exposed}\right) / Fe_{up|control},$$

where $Fe_{up}|_{control}$ and $Fe_{up}|_{exposed}$ are the concentrations of iron uptake 1 h after addition the Fe^{2+} ions in control and exposed samples, respectively. We found that the ability of ferritin to oxidize and store iron is reduced after being exposed to RF electromagnetic fields, that is, ΔFe_{uptake} is larger than 0. The change is a function of the molecular concentrations, exposure time and $\omega \bullet B$ product, where $\omega = 2\pi f$, and B is magnetic flux density of applied RF electromagnetic fields. The iron absorbed in 3.5 μM ferritin solutions exposed to RF field of 30 μT at 1 MHz for 5 h (total energy released ~ 35 JM^{-1}), is 20 ± 10% smaller than for control samples for added iron concentrations between 0.25 and 1 mM. In contrast, for the same condition in apoferritin (protein without inner ferrihydrite nanoparticles), the effect is not significant: ΔFe_{uptake} (apoferritin) = 1 ± 4%. The effect depends on the relative ferritin-iron concentrations, and it has not statistical significance for large Fe^{2+} concentrations (~1 mM). The fact that there is no effect in apoferritin reinforces our hypothesis that the mechanism of interaction is mediated by the nanoparticles: in proteins without a ferrihydrite core, there is no effect.

The fact that there is no effect in apoferritin reinforces our hypothesis that the mechanism of interaction is mediated by the nanoparticle: The inner superparamagnetic ferrihydrite nanoparticle increases its internal energy when exposed RF electromagnetic fields via Neel absorption/relaxation. This energy is irradiated to the surrounding protein cage, alternating the protein ability to uptake and release iron.

The effect is nonthermal and dependent on the frequency-amplitude product of the electromagnetic field and the relative concentrations of ferritin and the iron chelator. This effect may be used in iron biochemistry, and in calculations of the medical effects of environmental RF electromagnetic fields. In other words, our findings open a new path for the study of nonthermal bioeffects of RF electromagnetic fields at the molecular scale. We need in vivo studies to demonstrate the findings obtained by in vitro studies.

Although the described effects only happen at high ferritin concentrations not found in healthy organisms, individuals with high levels of iron (hemochromatosis) or exposed to high fields may be affected. Given the role of Fe^{2+} in oxidative processes via the Fenton reaction, a protein malfunction would have serious consequences. This could be at the origin of some RF electromagnetic field effects in oxidative stress related disorders.

Hemochromatosis, or hereditary hemochromatosis (HH), is an inherited autosomal recessive iron overload disorder resulting in the failure of the normal hepcidin response to body iron stores, leading to increased duodenal absorption of dietary iron. The increased iron enters the plasma and may be deposited in various target organs, particularly the liver, and may lead to clinical signs and symptoms (Kanwar & Kowdley, 2013). A healthy adult need between 10 mg (males) and 18 mg (females) of iron per day. About 1–2 mg of iron in the Fe^{2+} form is absorbed each day chiefly through villi in the duodenum to compensate for the 1–2 mg daily body loss of iron. Normal men absorb about 1 mg iron per day, menstruating women 2 mg iron per day, and hemochromatosis patients 2–5 mg iron per day (Walker et al., 1998). Iron is stored as ferritin, and each ferritin molecules can hold up to 4,500 iron ions in storage. It is estimated that 0.11 μg/L of plasma ferritin represents about 1 mg of stored iron. Normal iron storage is about 750–1,000 mg in men and 300–500 mg in women. Hemochromatosis patients may store 20–40 g of iron in storage organs. There are many attempts for the treatments of HH such as phlebotomy therapy and chelation therapy when serum ferritin (SF) concentration in patients falls in 300–1,000 μg/L or exceeds 1,000 μg/L. Our method may contribute to the treatment with respect to ferritin concentration in patients by exposures to RF magnetic fields. Further studies are required to obtain basic data and information, for example, as to what concentration of ferritin complexes would be needed.

We observed that colloidal solutions of magnetic nanoparticles 15–40 nm in size show optical fluorescence in the visible range at concentrations as low as a few μg/ml. Therefore, magnetic nanoparticles can be used for simultaneous imaging and displacement through the magnetophoresis of bioelements. Our efforts are also focused on the use of magnetic nanoparticles functionalized with cysteine and the peptide breaker iAβ5 for the imaging and dissolution of β-amyloid aggregation related to Alzheimer's disease (AD). The nanoparticles link to the specific β-sheet aggregation point of the amyloid and, given their magnetic properties, can be used as a contrast agent in MRI for the imaging of small amyloid deposits, or to break apart the amyloids via power loss. One of the main challenges of AD is the early detection of amyloid deposits. The functionalization of these deposits to magnetic nanoparticles would greatly facilitate their detection, making early treatment possible, and slow down the disease (Cespedes & Ueno, 2015; Ueno, 2012).

Amyloid imaging using positron emission tomography (PET) has an emerging role in the management of AD. The basis of this imaging is grounded on the fact that the hallmark of AD is the histological detection of beta amyloid plaques (Aβ) at postmortem autopsy (Suppiah et al., 2019). 2-Deoxy-2-[^{18}F] fluorodeoxyglucose ([^{18}F] FDG), a glucose analog, is utilized for PET brain imaging for the management of AD. Healthy brain cells avidly take up the substance, as they highly metabolized glucose, but the substance is relatively reduced in uptake in the temporo-parietal cortical regions that are affected by AD. Although the role of [18F] FDG has been established for making the diagnosis of AD, the accuracy of the scan interpretations can decline markedly when it involves older patients (Suppiah et al., 2019). Our proposed idea using magnetic nanoparticles may contribute to imaging of AD as a biomarker in MRI.

Our idea about potential physiological pathways for iron-related illnesses and the role of ferritin function is shown in Figure 10 (Cespedes & Ueno, 2015). Ferritin should oxidize Fe^{2+} and store it as Fe^{3+} in ferrihydrite, but if the iron cage protein is malfunctioning, Fe^{2+} can remain outside or not be oxidized during absorption. Fe^{2+} is then dangerous as it acts as pathway in the formation of free radicals. In healthy condition, however, the equilibrium between Fe^{2+} and Fe^{3+} is well balanced. RF electromagnetic fields would affect the equilibrium and nonequilibrium processes between Fe^{2+} and Fe^{3+} ions.

Given its relationship to oxidative stress and formation of free radicals, it has been speculated that the presence of iron in the brain could be associated to neurodegenerative disorders. Biomagnetite nanocrystals and ferrihydrite have been associated to AD (Everett et al., 2014). For example, the superior temporal gyrus brain tissue from patients with AD and age-matched control subjects shows an exponential correlation between the concentrations of the Fe^{2+} iron ion containing iron oxide, magnetite (Fe_3O_4), and the fraction of those particles that are smaller than 20 nm in diameter. There is also potential evidence of ferritin and/or its interaction with amyloids being at least partly responsible for the accumulation of Fe^{2+} that leads to early onset dementia and AD. A correlation between ferritin levels and onset of dementia has been studied (Bartzokis et al., 2004), although other factors, such as gender and age, make it difficult to find a straight correlation. The relationship between iron and dementia may simply be due to the role of iron in lipid peroxidation, for example, during the breaking of the cell membrane by β-amyloid in AD (Rottkamp et al., 2001).

Conditions such as neuroferritinopathy and Friedreich ataxia are associated with mutations in genes that encode proteins that are involved in iron metabolism, and as the brain ages, from accumulation in regions that are affected by Alzheimer's and Parkinson's disease. High concentrations of reactive Fe^{2+} can increase oxidative stress-induced neuronal vulnerability, and iron accumulation might increase the toxicity of the environment in neurodegenerative disorders (Zecca et al., 2004). To determine precisely the role of ferritin in these diseases, further methods to study and image the iron content in vivo would likely be needed, and also to separate iron in form of ferrihydrite within ferritin with free particles and/or stored in malfunctioning proteins with different oxidation states, that is as Fe^{2+} irons. Studying the accumulation and cellular distribution of iron during aging must be correlated also with protein and genomic deficiencies.

It is important to assess the safety of RF electromagnetic fields used for potential medical applications. Biological effects of RF electromagnetic fields are evaluated by specific absorption rate (SAR) absorbed in the living tissues defined by [W/kg]. We calculated SAR in ferritin iron absorbed by irradiation of 100 μT at various frequencies using the time scale for a ferrihydrite nanoparticle with Neel relaxation time $\tau_N = 0.13$ ns. The denaturation limit by heat assumes that all the power dissipated is absorbed by the protein, which is not likely and would need to be probed experimentally. The heat rate limit is 1.6 [W/kg] over 100 g, or, 1–10 mg ferritin iron per 100 g of

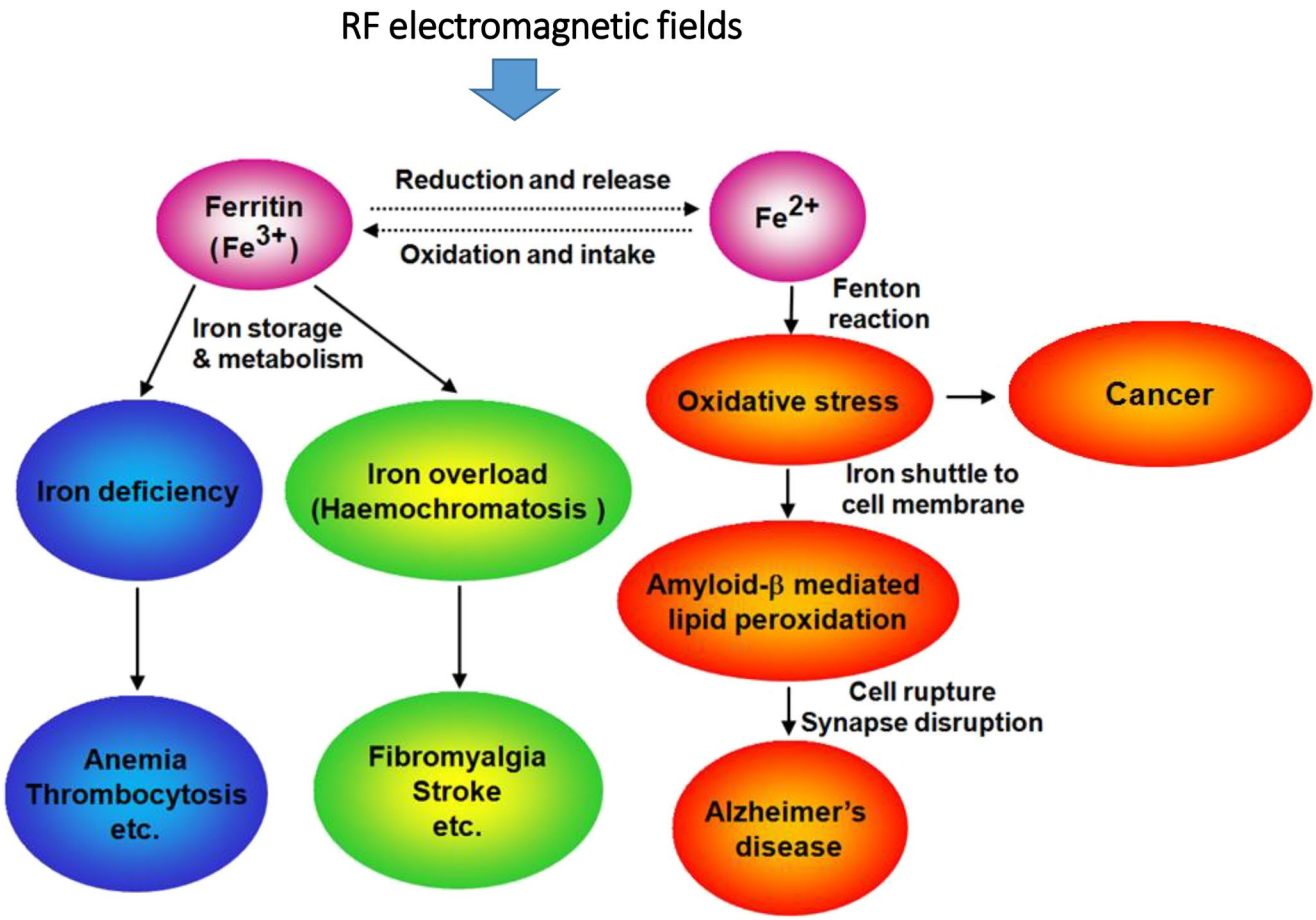

Figure 10. Potential physiological pathways for iron-related illnesses and the role of ferritin function (Cespedes & Ueno, 2015). Ferritin should oxidize Fe^{2+} and store it as Fe^{3+} in ferrihydrite. If the protein is malfunctioning, Fe^{2+} can remain outside or not be oxidized during absorption. Fe^{2+} is then dangerous as it acts as pathway in the formation of free radicals. RF electromagnetic fields would affect the equilibrium between Fe^{2+} and Fe^{3+}.

tissue. SAR absorbed in ferritin iron exposed to RF field of 100 μT at 1 MHz is around 0.01 [W/kg] in human spleen ferritin. We do not think it is likely that the effect could cause macroscopic heating in addition to the heat generated by artificial nanoparticles, due to the relatively low ferritin iron concentrations; in the brain, the maximum is of some 200 ng/g of tissue, found in the globus pallidus. Therefore, exposures to 1 MHz and 30 μT RF electromagnetic fields are safe.

From the point of view of RF effects, we have seen no evidence, at least at the amplitude and frequencies we have used, that the functioning of ferritin could result in an increased release of harmful iron ions. On the contrary, it would seem that iron release is slowed by the RF electromagnetic fields more significantly than iron absorption, which would result in a net iron deficiency for the experimental conditions and chemicals used. Even then, the concentrations used for our study are order of magnitude above those found in any healthy organism. However, studies into the form of the iron stored (i.e., the oxidation state), the size, and the composition of the particles and exposures under different exposure conditions would be needed. Furthermore, therapies to regulate iron biochemistry using RF electromagnetic fields could be considered.

7. Conclusions

We summarize three themes of the studies: electromagnetic brain stimulation (called TMS), MRI, and potential medical therapy by electromagnetics.

TMS with a figure-eight coil for localized stimulation of the brain has been proposed to study the functional organization of the human brain. Different coil configurations have been proposed for deep brain stimulation.

Further studies are needed for deep TMS with better focality. TMS has the potential to treat ailments such as depression and has a use in rehabilitation medicine. To obtain the basic understanding of the mechanisms for potential treatments of brain diseases, we studied the effect of repetitive TMS (rTMS) on neuronal electrical activities in the rat hippocampus, focusing on longterm potentiation. The results suggest that rTMS contributes to learning and memory, neuronal plasticity, recovery of injured neurons, and acquisition of tolerance against cerebral ischemia.

Imaging of electric impedance or conductivity in the brain based on MRI, called impedance MRI, are discussed. We proposed three different methods for impedance MRI. Among them, a conductivity MRI based on diffusion tensor MRI is a promising method to obtain the information of anisotropy caused by alignment of neuronal fibers in the brain. MRI of electric current in the brain were also investigated. We studied the sensitivity of MRI to magnetic fields. The results show that the theoretical sensitivity for magnetic fields in the brain is approximately 10^{-8} T. We measured MRI signals in the rat brain responded to electrical stimulation of the sciatic nerves. Transient changes in the signal intensity resulting from neuronal activities in the rat brain were measured. Molecular imaging based on MRI was also reviewed. CEST imaging is a novel MRI-based molecular imaging, and APT imaging is a promising molecular imaging because of its higher contrast effect compared with other imaging methods in CEST. Problems and limits for clinical use of CEST imaging were discussed.

Cancer cell destruction by electromagnetic force, acceleration of bone growth and nerve regeneration by strong magnetic fields, and effects of radio frequency electromagnetic fields on iron release and uptake from and into iron cage proteins, ferritins, were studied: TCC-S leukemic cells were combined with magnetizable beads by an antigen-antibody reaction. The CD33 antigen was expressed on the surface of TCC-S cells. After combination, the cell/beads/antibody complexes were stimulated by a coil that produced pulsed magnetic fields of 2.0 T with a field gradient of 100 T/m. The cancer cells were destroyed by the penetration of the beads into the cancer cells or the rupturing of cancer cells by the beads. We succeeded in bone growth acceleration using a bone morphogenetic protein 2 (BMP-2) exposed to an 8 T magnetic field during the early stage of bone formation. We also obtained that sciatic nerve regeneration of rats under the condition of transected sciatic nerves was accelerated by magnetic field exposures via magnetic orientation of type I collagen mixed as a scaffold. Finally, we observed novel effects that iron ion release and uptake from and into iron cage proteins, ferritins, were affected by exposures of RF electromagnetic fields of 1 MHz and 30 μT for 5 h. Possibilities of applications of these effects to diagnosis and treatments of brain diseases such as Alzheimer's disease were discussed.

These electromagnetic techniques are leading medicine and biology into a new horizon today and in the future.

Data Availability Statement

The data archiving is ready in the UTokyo Repository at the University of Tokyo, Tokyo, Japan. The URL is http://hdl.handle.net/2261/00079730 in https://repository.dl.itc.u-tokyo.ac.jp/?lang=english.

Acknowledgments
The studies were supported by many grants which include Grant-in-Aid for Specially Promoted Research, Ministry of Education, Science, Sports, Culture and Technology, Japan (No. 12002002) and Grant-in-Aid for Scientific Research (S) (No. 17100006) from Japan Society for the Promotion of Science (JSPS). The author thanks his coworkers, graduate students, and post-Doc., in particular, Drs. T. Tashiro, K. Iramina, T. Matsuda, O. Hiwaki, M. Fujiki, T. Yoshiura, M. Iwasaka, N. Iriguchi, M. Sekino, H. Kotani, M. Ogiue-Ikeda, S. Yamaguchi-Sekino, Y. Eguchi, M. Lu, and O. Cespedes, for their participation and collaborations.

References

Barker, A. T., Jalinous, R., & Freeston, I. L. (1985). Non-invasive magnetic stimulation of human motor cortex. *The Lancet*, *i*, 1325–1326.

Bartzokis, G., Tishler, T. A., Shin, I.-S., Lu, P. H., & Cummings, J. L.,(2004). Brain ferritin iron as a risk factor for age at onset in neurodegenerative diseases. *Annals of the New York Academy of Sciences*, *1012*, 224–236. https://doi.org/10.1196/annals.1306.019

Cespedes, O., Inomoto, O., Kai, S., Nibu, Y., Yamaguchi, T., Sakamoto, N., et al. (2010). Radio frequency magnetic field effects on molecular dynamics and iron uptake in cage proteins. *Bioelectromagnetics*, *31*, 311–317.

Céspedes, O., & Ueno, S. (2009). Effects of radio frequency magnetic fields on iron release from cage proteins. *Bioelectromagnetics*, *30*, 336–342. https://doi.org/10.1002/bem.20488

Cespedes, O., & Ueno, S. (2015). Effects of radio frequency magnetic fields on iron release and uptake from and into cage proteins. In S. Ueno, & M. Sekino, (Eds.), *Biomagnetics: Principles and applications of biomagnetic stimulation and imaging* (Chapter 8, pp. 219–257). CRC Press Taylor & Francis Group.

Crowther, L. J., Marketos, P., Williams, P. I., Melikhov, Y., & Jiles, D. C. (2011). Transcranial magnetic stimulation: Improved coil design for deep brain investigation. *Journal of Applied Physics*, *109*, 07B314. https://doi.org/10.1063/1.3563076

d'Arsonval, J. A. (1896). Dispositifs pour la mesure des courants alternatifs de toutes frequences. *Comptes Rendus de l'Académie des Sciences*, *48*, 450–451.

Frei, H. H. (Ed.), (1970). Introduction to the symposium on application of magnetism and bioengineering. *IEEE Transactions on Magnetics*, *MAG 6*, 307–375.

Eguchi, Y., Ohtori, S., Sekino, M., & Ueno, S. (2015). Effectiveness of magnetically aligned collagen for neural regeneration in vitro and in vivo. *Bioelectromagnetics*, *36*, 233–243. https://doi.org/10.1002/bem.21896

Everett, J., Céspedes, E., Shelford, L. R., Exley, C., Collingwood, J. F., Dobson, J., et al. (2014). Evidence of redox-active iron formation following aggregation of ferrihydrite and the Alzheimer's disease peptide β-amyloid. *Inorganic Chemistry*, *53*, 2803–2809. https://doi.org/10.1021/ic402406g

Fujiki, M., & Stewart, O. (1997). High frequency transcranial magnetic stimulation for protection against delayed neuronal death induced by transient ischemia. *Journal of Neurosurgery*, *99*, 1063–1069.

Gilbert, W. (1600). *De Magnete. Translation to English by Mottelay (1958)*. Dover. https://doi.org/10.5479/sil.113709.39088016899940

Grossman, N., Bono, D., Dedic, N., Kodandaramaiah, S. B., Rudenko, A., Suk, H.-J., et al. (2017). Noninvasive deep brain stimulation via temporally interfering electric fields. *Cell*, *169*, 1029–1041. https://doi.org/10.1016/j.cell.2017.05.024

Hatada, T., Sekino, M., & Ueno, S. (2005). Finite element method-based calculation of the theoretical limit of sensitivity for detecting weak magnetic fields in the human brain using magnetic-resonance imaging. *Journal of Applied Physics*, *97*, 10E109. https://doi.org/10.1063/1.1861553

Kamei, H., Iramina, K., Yoshikawa, K., & Ueno, S. (1999). Neuronal current distribution imaging using magnetic resonance. *IEEE Transactions on Magnetics*, *35*, 4109–4111. https://doi.org/10.1109/20.800771

Kanwar, P., & Kowdley, K. V. (2013). Diagnosis and treatment of hereditary hemochromatosis: An update. *Expert Review of Gastroenterology & Hepatology*, *7*(6), 517–530. www.expert-reviews.com. https://doi.org/10.1586/17474124.2013.816114

Kotani, H., Kawaguchi, H., Shimokawa, T., Iwasaka, M., Ueno, S., Ozawa, H., et al. (2002). Strong static magnetic field stimulates bone formation to a definite orientation *in vivo* and *in vitro*. *Journal of Bone and Mineral Research*, *17*, 1814–1821.

Lauterbur, P. C. (1973). Image formation by induced local interactions: Examples employing nuclear magnetic resonance. *Nature*, *242*(5394), 190–191. https://doi.org/10.1038/242190a0

Lee, J.-S., Xia, D., Jerschow, A., & Regatta, R. R. (2015). *In vitro* study of endogenous CEST agents at 3 T and 7 T. *Contrast Media and Molecular Imaging*, *11*(1), 1–26. https://doi.org/10.1002/cmmi.1652

Lu, M., & Ueno, S. (2015). Computational study toward deep transcranial magnetic stimulation using coaxial circular coils. *IEEE Transactions on Biomedical Engineering*, *62*(12), 2911–2919. https://doi.org/10.1109/tbme.2015.2452261

Lu, M., & Ueno, S. (2017). Comparison of the induced fields using different coil configurations during deep transcranial magnetic stimulation. *PLoS One*, *12*(6), 1–12.e0178422.

Mansfield, P. (1977). Multi-planar image formation using NMR spin echoes. *Journal of Physics C: Solid State Physics*, *10*, L55–L58. https://doi.org/10.1088/0022-3719/10/3/004

Müller, M., Toschi, N., Kresse, A. E., Post, A., & Keck, M. E. (2000). Long-term repetitive transcranial magnetic stimulation increases the expression of brain-derived neurotrophic factor and cholecystokinin mRNA, but not neuropeptide tyrosine mRNA in specific areas of rat brain. *Neuropsychopharmacology*, *23*, 205–215. https://doi.org/10.1016/s0893-133x(00)00099-3

Ogawa, S., Lee, T. M., Kay, A. R., & Tank, D. W. (1990). Brain magnetic resonance imaging with contrast dependent on blood oxygenation. *Proceedings of the National Academy of Sciences*, *87*(24), 9868–9872. https://doi.org/10.1073/pnas.87.24.9868

Ogawa, S., Tank, D. W., Menon, R., Ellermann, J. M., Kim, S. G., Merkle, H., & Ugurbil, K. (1992). Intrinsic signal changes accompanying sensory stimulation: Functional brain mapping with magnetic resonance imaging. *Proceedings of the National Academy of Sciences*, *89*(13), 5951–5955. https://doi.org/10.1073/pnas.89.13.5951

Ogiue-Ikeda, M., Kawato, S., & Ueno, S. (2003). The effect of repetitive transcranial magnetic stimulation on long-term potentiation in rat hippocampus depends on stimulus intensity. *Brain Research*, *993*, 222–226. https://doi.org/10.1016/j.brainres.2003.09.009

Ogiue-Ikeda, M., Kawato, S., & Ueno, S. (2005). Acquisition of ischemic tolerance by repetitive transcranial magnetic stimulation in the rat hippocampus. *Brain Research*, *1037*, 7–11. https://doi.org/10.1016/j.brainres.2004.10.063

Ogiue-Ikeda, M., Sato, Y., & Ueno, S. (2003). A new method to destruct targeted cells using magnetizable beads and pulsed magnetic force. *IEEE Transactions on Nanobioscience*, 2(4), 262–265. https://doi.org/10.1109/tnb.2003.820276

Roth, Y., Zangen, A., & Hallett, M. (2002). A coil design for transcranial magnetic stimulation of deep brain regions. *Journal of Clinical Neurophysiology*, *19*, 361–370. https://doi.org/10.1097/00004691-200208000-00008

Rottkamp, C. A., Raina, A. K., Zhu, X., Gaier, E., Bush, A. I., Atwood, C. S., et al. (2001). Redox-active iron mediates amyloid-β toxicity. *Free Radical Biology and Medicine*, *30*, 447–450. https://doi.org/10.1016/s0891-5849(00)00494-9

Sekino, M., Inoue, Y., & Ueno, S. (2005). Magnetic resonance imaging of electrical conductivity in the human brain. *IEEE Transactions on Magnetics*, *41*, 4203–4205. https://doi.org/10.1109/tmag.2005.854804

Sekino, M., Ohsaki, H., Yamaguchi-Sekino, S., Iriguchi, N., & Ueno, S. (2009). Low-frequency conductivity tensor of rat brain tissues inferred from diffusion MRI. *Bioelectromagnetics*, *30*, 489–499. https://doi.org/10.1002/bem.20505

Sekino, M., Ohsaki, H., Yamaguchi-Sekino, S., & Ueno, S. (2009). Toward detection of transient changes in magnetic-resonance signal intensity arising from neuronal electrical activities. *IEEE Transactions on Magnetics*, *45*, 4841–4844. https://doi.org/10.1109/tmag.2009.2022954

Stefanini, S., Cavallo, S., Wang, C.-Q., Tataseo, P., Vecchini, P., Giartosio, A., & Chiancone, E. (1996). Thermal stability of horse spleen apoferritin and human recombinant H apoferritin. *Archives of Biochemistry and Biophysics*, *325*, 58–64. https://doi.org/10.1006/abbi.1996.0007

Stejskal, E. O., & Tanner, J. E. (1965). Use of spin echo in pulsed magnetic field gradient to study anisotropic, restricted diffusion and flow. *The Journal of Chemical Physics*, *43*, 3579–3603. https://doi.org/10.1063/1.1696526

Suppiah, S., Didier, M.-A., & Vinjamuri, S. (2019). The who, when, why, and how of PET amyloid imaging in management of Alzheimer's disease—Review of literature and interesting images. *Diagnostics*, *9*(2), 65–24. https://doi.org/10.3390/diagnostics9020065

Togao, O., Yoshiura, T., Keupp, J., Hiwatashi, A., Yamashita, K., Kikuchi, K., et al. (2014). Amide proton transfer imaging of adult diffuse gliomas: Correlation with histopathological grades. *Neuro-Oncology*, *16*(3), 441–448. https://doi.org/10.1093/neuonc/not158

Torbet, J., Freyssinet, J.-M., & Hudry-Clergeon, G. (1981). Oriented fibrin gels formed by polymerization in strong magnetic fields. *Nature*, *289*, 91–93. https://doi.org/10.1038/289091a0

Ueno, S. (1994). Focal and vectorial magnetic stimulation of the human brain. In S. Ueno, (Ed.), *Biomagnetic stimulation* (pp. 29–47). Plenum Press. https://doi.org/10.1007/978-1-4757-9507-3_3

Ueno, S. (2012). Studies on magnetism and bioelectromagnetics for 45 years: From magnetic analog memory to human brain stimulation and imaging. *Bioelectromagnetics*, *33*(1), 3–22. https://doi.org/10.1002/bem.20714

Ueno, S. (2015). Introduction. In S. Ueno, & M. Sekino, (Eds.), *Biomagnetics: Principles and applications of biomagnetic stimulation and imaging* (Chapter 1, pp. 1–22). CRC Press Taylor & Francis Group. https://doi.org/10.1201/b18831-2

Ueno, S. (2020). *Bioimaging: Imaging by light and electromagnetics in medicine and biology* (pp. 1–268). CRC Press Taylor & Francis Group.

Ueno, S., & Fujiki, M. (2007). Magnetic stimulation. In W. Andra, & H. Nowak (Eds.), *Magnetism in medicine: A handbook* (2nd ed. Chapter 4.4, pp. 511–528). Wiley-VCH verlag GmbH & KGaA.

Ueno, S., & Iriguchi, N. (1998). Impedance magnetic resonance imaging: A method for imaging of impedance distributions based on magnetic resonance imaging. *Journal of Applied Physics*, *83*, 6450–6452. https://doi.org/10.1063/1.367599

Ueno, S., & Iwasaka, M. (1994). Properties of diamagnetic fluid in high gradient magnetic fields. *Journal of Applied Physics*, *75*, 7177–7179. https://doi.org/10.1063/1.356686

Ueno, S., Matsuda, T., & Fujiki, M. (1990). Functional mapping of the human motor cortex obtained by focal and vectorial magnetic stimulation of the brain. *IEEE Transactions on Magnetics*, *26*, 1539–1544. https://doi.org/10.1109/20.104438

Ueno, S., Tashiro, T., & Harada, K. (1988). Localized stimulation of neural tissues in the brain by means of a paired configuration of time-varying magnetic fields. *Journal of Applied Physics*, *64*, 5862–5864. https://doi.org/10.1063/1.342181

Van Zijl, P. C. M., & Yadav, N. N. (2011). Chemical exchange saturation transfer (CEST): What is in a name and what isn't? *Magnetic Resonance in Medicine*, *65*(4), 927–948. https://doi.org/10.1002/mrm.22761

Walker, E. M., Jr, Wolfe, M. D., Norton, M. N., Walker, S. M., & Jones, M. M. (1998). Hereditary hemochromatosis. *Annals of Clinical and Laboratory Science*, *28*(5), 300–312.

Ward, K. M., Aletras, A. H., & Balaban, R. S. (2000). A new class of contrast agents for MRI based on proton chemical exchange dependent saturation transfer (CEST). *Journal of Magnetic Resonance*, *143*(1), 79–87. https://doi.org/10.1006/jmre.1999.1956

Yau, S.-T., Petsev, D. N., Thomas, B. R., & Vekilov, P. G. (2000). Molecular-level thermodynamic and kinetic parameters for the self-assembly of apoferritin molecules into crystals. *Journal of Molecular Biology*, *303*, 667–678. https://doi.org/10.1006/jmbi.2000.4171

Yoshiura, T. (2020). Chemical exchange saturation transfer and amide proton transfer imaging. In S. Ueno (Ed.), *Bioimaging: Imaging by light and electromagnetics in medicine and biology* (Chapter 5, pp. 101–120). CRC Press Taylor & Francis Group. https://doi.org/10.1201/9780429260971-5

Yukawa, Y., Iriguchi, N., & Ueno, S. (1999). Impedance magnetic resonance imaging with external AC field added to main static field. *IEEE Transactions on Magnetics*, *35*, 4121–4123. https://doi.org/10.1109/20.800775

Zangen, A., Roth, Y., Voller, B., & Hallett, M. (2005). Transcranial magnetic stimulation of deep brain regions: Evidence for efficacy of the H-coil. *Clinical Neurophysiology*, *116*, 775–779. https://doi.org/10.1016/j.clinph.2004.11.008

Zecca, L., Youdim, M. B. H., Riederer, P., Connor, J. R., & Crichton, R. R. (2004). Iron, brain aging and neurodegenerative disorders. *Nature Reviews Neuroscience*, *5*, 863–873. https://doi.org/10.1038/nrn1537

Zhou, J., Lal, B., Wilson, D. A., Laterra, J., & van Zijl, P. C. M. (2003). Amide proton transfer (APT) contrast for imaging of brain tumors. *Magnetic Resonance in Medicine*, *50*, 1120–1126. https://doi.org/10.1002/mrm.10651